[5] *Nationwide Ocean Wave Information Network for Ports and Harbours (NOWPHAS) 1993*, Ports and Harbours Construction Bereau, Ministry of Transport, Ed., Tokyo, Japan: Coastline Development and Technology Research Center, 1994.
[6] Y. Nemote, H. Nishino, M. Ono, H. Mizutamari, K. Nishikawa, and K. Tanaka, "Japanese earth resources satellite-1 synthetic aperture radar," *Proc. IEEE*, vol. 79, pp. 800–809, 1991.
[7] K. Ouchi, "On the multilook images of moving targets by synthetic aperture radars," *IEEE Trans. Antennas Propagat.*, vol. AP-33, pp. 823–827, 1985.
[8] ——, "Multilook images of ocean waves by synthetic aperture radars," *IEEE Trans. Antennas Propagat.*, vol. AP-35, pp. 313–318, 1987.
[9] K. Ouchi and H. Mitsuyasu, "Detection and analysis of oceanic internal waves by JERS-1 SAR," *Proc. Remote Sens. Conf. Japan*, 1997, pp. 113–116, 1997.
[10] R. K. Raney, P. Vachon, R. A. De Abreu, and A. S. Bhogal, "Airborne SAR observation of ocean surface waves penetrating floating ice," *IEEE Trans. Geosci. Remote Sensing*, vol. 27, pp. 492–500, 1989.
[11] R. K. Raney and P. W. Vachon, "SAR imaging of ocean waves: Some observations from LIMEX/LEWEX '87," in *Directional Ocean Wave Spectra*, R. Beal, Ed. Baltimore, MD/London, U.K.: Johns Hopkins Univ. Press, 1991.
[12] P. W. Vachon and R. K. Raney, "Resolution of the ocean wave propagation direction in SAR imagery," *IEEE Trans. Geosci. Remote Sensing*, vol. 29, pp. 105–112, 1991.
[13] P. W. Vachon, R. K. Raney, and A. S. Bhogal, "SAR and spectral processing for ocean waves: experimental results," in *Proc. GARSS'90*, 1990, pp. 1447–1450.
[14] P. W. Vachon and J. C. West, "Spectral estimation techniques for multilook SAR images of ocean waves," *IEEE Trans. Geosci. Remote Sensing*, vol. 30, pp. 568–577, 1992.
[15] I. R. Young, W. Rosenthal, and F. Ziemer, "A three-dimensional analysis of marine radar images for the determination of ocean wave directionality and surface currents," *J. Geophys. Res.*, vol. 90, no. C1, pp. 1049–1059, 1985.

Deconvolution of Seismic Data Using Adaptive Gaussian Mixtures

Ignacio Santamaría, Carlos J. Pantaleón, Jesús Ibáñez, and Antonio Artés

***Abstract*— Based on a Gaussian mixture model for the reflectivity sequence, we present a new technique for blind deconvolution of seismic data. The method obtains a deconvolution filter that maximizes at its output a measure of the relative entropy between the proposed Gaussian mixture and a pure Gaussian distribution. A new updating procedure for the mixture parameters is included in the algorithm: it allows us to apply the algorithm without any prior knowledge about the signal and noise. A simulation example illustrates the performance of the proposed method.**

***Index Terms*—Deconvolution, estimation, iterative methods, seismology.**

I. Introduction

In seismic deconvolution, it is generally recognized that the reflectivity can be represented by a sparse spike train: each reflector stands for a change in the acoustic impedance at the layer interfaces. A typical model for the reflectivity is the Bernoulli–Gaussian (BG) model [1], for which the signal follows a Gaussian distribution with probability λ, and its value is zero with probability $1-\lambda$.

For deconvolution of BG signals, a commonly used technique consists of maximizing a global likelihood function to obtain the nonzero positions and their amplitudes, the BG model parameters, and possibly the distorting linear system. However, the proposed maximization approaches [1], [2] have a high computational cost mainly due to the detection part of the problem (i.e., the Bernoulli part of the model).

In the present work, we consider a Gaussian mixture model for the reflectivity sequence in the context of iterative seismic deconvolution. In particular, we assume that the prior distribution of the reflection coefficient sequence can be approximated with a mixture of a narrow and a broad zero-mean Gaussian. This model offers some advantages when compared to the BG model: first, unlike the BG model, it accounts for the diffraction effects that produce a scattering noise added to the sparse reflectivity signal. That is, with the proposed model, the narrow Gaussian models the smaller reflectors due to backscattering as well as the noise, whereas the broad one models the mayor layering effects. It is also possible to include these scattering effects in the BG model by adding a zero-mean Gaussian sequence [1], but then the likelihood function turns even harder to maximize.

Second, the BG model can be considered as a particular case of the Gaussian mixture: when the variance of the narrow Gaussian approaches zero, the Gaussian mixture model approaches a BG distribution.

Finally, when we consider iterative deconvolution approaches, at each iteration we obtain a new inverse filter such that the convolution with the seismic data results in the complete or partial removal of the distorting linear filter. Therefore, the output of the deconvolution filter can be modeled again as a Gaussian mixture [3]. In this case, the narrow Gaussian models not only the backscattering noise, but the convolutional noise, which accounts for an incomplete removal of the distorting filter.

Based on a Gaussian mixture model, Godfrey and Rocca proposed the zero-memory nonlinear deconvolution method [3] (also called Bussgang method [4]). At each iteration, this technique obtains rough estimates of the reflectivity by means of a matched nonlinear function. This estimate is cross correlated with the observations, and a new deconvolution filter is obtained. From the deconvolved signal, a new reflectivity is estimated and the procedure is iterated until convergence. In [3], the parameters of the mixture and therefore the nonlinear estimator are fixed in advance.

In this paper, we proposed a new blind deconvolution approach for seismic data that is also based on a Gaussian mixture model for the reflectivity. The deconvolution filter maximizes at its output a measure of the relative entropy between the assumed Gaussian mixture and a single Gaussian having the same variance as the data. The maximization procedure leads to a new nonlinear estimator for the input signal. At each iteration, the mixture parameters are reestimated to fit the distribution of the estimated reflectivity.

II. New Inverse Filter Criterion for Seismic Deconvolution

In seismic exploration, it is customary to consider the following convolutional model for the observed seismic data $\{z_i\}$:

$$\{z_i\} = \{x_i\} * \{h_i\} + \{n_i\} \tag{1}$$

Manuscript received August 13, 1996; revised October 27, 1997.

I. Santamaría, C. J. Pantaleón, and J. Ibáñez are with DICOM, ETSII y Telecomunicación, University of Cantabria, 39005 Santander, Spain (e-mail: nacho@gtas.dicom.unican.es).

A. Artés is with DSSR, ETSI Telecomunicación, UPM, Ciudad Universitaria s/n, 28040 Madrid, Spain (e-mail: antonio@gtts.ssr.upm.es).

Publisher Item Identifier S 0196-2892(99)00837-2.

where $\{x_i\}$ is the reflectivity, $\{h_i\}$ is a linear time-invariant and possibly nonminimum-phase system (seismic wavelet), $\{n_i\}$ models the noise, and $*$ denotes convolution.

We assume that the probability distribution function (pdf) of the reflectivity can be approximated with a mixture of a narrow (subscript 1) and a broad (subscript 2) zero-mean Gaussian

$$p(x) = \frac{\pi_1}{\sqrt{2\pi}\sigma_1} e^{-(x^2/2\sigma_1^2)} + \frac{\pi_2}{\sqrt{2\pi}\sigma_2} e^{-(x^2/2\sigma_2^2)} \tag{2}$$

where π_1 and π_2 are the mixing proportions and they are therefore, constrained to sum 1.

Given a set of N samples of the reflectivity generated according to the previous model $\{x_1, \cdots, x_N\}$, and denoting each component of the mixture as G_j, the detection part of the problem consists of determining the posterior probabilities $p(G_j|x_i)$, which are given by

$$p(G_j|x_i) = r_j(x_i) = \frac{\pi_j p_j(x_i)}{\sum_k \pi_k p_k(x_i)}, \qquad j = 1, 2 \tag{3}$$

where $p_j(x_i)$ is the probability density of x_i under Gaussian j, i.e.,

$$p_j(x_i) = \frac{1}{\sqrt{2\pi}\sigma_j} \exp -\left(\frac{x_i^2}{2\sigma_j^2}\right). \tag{4}$$

The object of seismic deconvolution is to obtain an inverse filter $\{f_i\}$, such that the convolution of $\{f_i\}$ with the seismogram $\{z_i\}$ removes the distorting wavelet and the noise. On the other hand, as it is shown in [5], convolution always increases the Gaussian character of the pdf; therefore, the deconvolution filter should remove this effect by making its output to fit (2) again. For doing so, we propose to obtain an inverse filter that maximizes at its output a measure of the relative entropy between mixture model (2) and a single Gaussian distribution having the same variance, i.e.,

$$J = \sum_i \log \sum_j \pi_j p_j(y_i) - \sum_i \log f(y_i) \tag{5}$$

where $p_j(y_i)$ is the probability density of y_i under Gaussian j in the mixture and $f(y_i)$ is a Gaussian pdf with variance $\sigma^2 = \pi_1\sigma_1^2 + \pi_2\sigma_2^2$. This objective function is used to drive the pdf of the inverse filter's output away from the initial Gaussian distribution toward the assumed Gaussian mixture model.

The maximization of (5) with respect to the filter coefficients gives

$$\frac{\partial J}{\partial f_m} = \sum_i \left\{ \frac{y_i}{\sigma^2 \sum_j \frac{r_j(y_i)}{\sigma_j^2}} - y_i \right\} \frac{\partial y_i}{\partial f_m} = 0 \tag{6}$$

where the factors $r_j(y_i)$ are the posterior probabilities given by (3).

Considering a deconvolution filter of length $L+1$ and a sequence of observations $\{z_i\}$ of length M, we have

$$y_i = \sum_{j=0}^{L} f_j z_{i-j}, \qquad i = 0, \cdots, N-1 \tag{7}$$

where $N = M + L$.

Therefore, $\partial y_i / \partial f_m = z_{i-m}$ and substituting (7) for the rightmost y_i term in (6), we obtain

$$\sum_l f_l \sum_i z_{i-l} z_{i-m} = \sum_i \frac{y_i}{\sigma^2 \sum_j \frac{r_j(y_i)}{\sigma_j^2}} z_{i-m}. \tag{8}$$

The set of equations (8) can be written in matrix notation as

$$\mathbf{R}_{zz}\mathbf{f} = \mathbf{g} \tag{9}$$

where $\mathbf{R}_{zz}$ is the Toeplitz autocorrelation matrix of the observations and $\mathbf{g}$ is the cross-correlation vector between the observations and a nonlinear estimate of the input signal, which is given by

$$\hat{x} = g(y) = \frac{y}{\sigma^2 \sum_j \frac{r_j(y)}{\sigma_j^2}}. \tag{10}$$

The set of equations (9) can be solved using the iterative procedure proposed in [3]: starting from an initial inverse filter, an estimate of the input signal is obtained using (10); this new estimate is cross correlated with the observations, and a new inverse filter is obtained solving (9). At each iteration the energy of the estimated signal must be normalized to a fixed value. This procedure is iterated until convergence is obtained.

III. Nonlinearity Optimization

A complete application of the proposed method requires a careful selection of the parameters defining the mixture model and therefore the nonlinearity. Conventional Bussgang approaches use a fixed nonlinearity: for instance, in [3] from the three parameters defining the Gaussian mixture, the ratio between the variances $S = \sigma_2^2/\sigma_1^2$ and the proportion of the broad Gaussian π_2 are fixed in advance (independent of iteration). To make the algorithm data dependent, the variance of the estimated signal after each iteration must be equal to the mixture variance: this provides an additional constraint to get the mixture parameters.

To avoid this *a priori* selection, in this paper, we propose a method to update the mixture parameters and, therefore, the nonlinear function $g(y)$, at each step of the deconvolution process. This updating procedure has been previously applied to nonblind deconvolution problems [6].

The key idea of the method is to obtain a maximum likelihood estimate of the mixture parameters $\theta = (\pi_1, \sigma_1, \pi_2, \sigma_2)$ for each new estimate of the reflectivity signal. These estimates can be obtained applying the expectation-maximization (EM) algorithm [7].

Let us start by defining the observed incomplete data as the estimate of the reflectivity obtained from (10) after iteration k: $\{\hat{x}_k\}$. On the other hand, the unobserved data are given by $\chi = (\mathbf{d}_1, \mathbf{d}_2)$, where $\mathbf{d}_j$, $j = 1, 2$ are vectors of Bernoulli random variables. The ith element of $\mathbf{d}_j$ selects the Gaussian associated to the ith sample, i.e.,

$$d_{j,i} = \begin{cases} 1; & \text{if } x_i \in G_j \\ 0; & \text{if } x_i \notin G_j. \end{cases} \tag{11}$$

Using this particular choice for the complete data $(\{\hat{x}_k\}, \mathbf{d}_1, \mathbf{d}_2)$, and denoting the current estimate of θ after k iterations of the EM algorithm as θ_k, it is easy to see that the E-step of the next iteration is given by

$$E[d_{j,i}|\{\hat{x}_k\}, \theta_k] = r_j(\hat{x}_{i,k}) \tag{12}$$

where $E[\cdot]$ denotes expectation. Therefore, the E-step is equivalent to recomputing the posterior probabilities for the estimated signal.

Once $r_j(\hat{x}_{i,k})$ is known, in the M-step, we maximize J with respect to θ; taking the derivative and equating it to zero gives

$$\sigma_{j,k+1}^2 = \frac{\sum_i \hat{x}_{i,k}^2 r_j(\hat{x}_{i,k})}{\sum_i r_j(\hat{x}_{i,k})} \tag{13}$$

$$\pi_{j,k+1} = \frac{1}{N} \sum_i r_j(\hat{x}_{i,k}). \tag{14}$$

It is known that the convergence rate of the EM algorithm may be slow; to avoid this problem, we propose the following modification:

after each new $\{\hat{x}_k\}$ is obtained, only one iteration of the EM algorithm is carried out to obtain a new estimate of θ.

On the other hand, note that each new estimate of θ changes the cost function; therefore, to avoid instability, it is important to force a slow change in the parameters of the mixture. For this reason, we choose the following updating procedure:

$$\sigma^2_{j,\,k+1} = \gamma\sigma^2_{j,\,k} + (1-\gamma)\frac{\sum_i \hat{x}^2_{i,k} r_j(\hat{x}_{i,k})}{\sum_i r_j(\hat{x}_{i,k})} \tag{15}$$

$$\pi_{j,\,k+1} = \gamma\pi_{j,\,k} + (1-\gamma)\frac{1}{N}\sum_i r_j(\hat{x}_{i,\,k}) \tag{16}$$

γ being a constant such that $0.8 < \gamma < 0.95$.

In fact, note that from four parameters in θ only two must be estimated in each iteration since $\pi_2 = 1-\pi_1$ and one of the variances is fixed by the following constraint

$$\sigma^2_{x,\,k} = \pi_1\sigma^2_1 + \pi_2\sigma^2_2 \tag{17}$$

where $\sigma^2_{x,\,k}$ is the variance of the estimate $\hat{x}$ at iteration k.

This updating procedure allows the starting of the algorithm with a very soft nonlinearity and, progressively, the increasing of the nonlinear character of the estimator as iteration proceeds. In this way, the proposed algorithm has a greater flexibility than Godfrey's approach [3], which uses a fixed nonlinearity.

On the other hand, if we are looking for a fully sparse reflectivity, the final nonlinearity can be used as a detector; this is important in high noise situations since, in these cases, the deconvolution filter is unable to remove completely the forward distorting filter while simultaneously eliminating the noise. Using the proposed approach, the partial removal of the forward filter can be corrected after the nonlinearity.

Finally, the proposed algorithm can be summarized in the following steps.

1) Initialize the mixture parameters $\pi_{j,\,0}$, $\sigma_{j,\,0}$, $j = 1, 2$. A reasonable mixture initialization could be $\pi_1 = \pi_2 = 0.5$ and $\sigma^2_2 > \sigma^2_1$, with σ^2_1 being a small fraction of the observations variance σ^2_z. These mixture parameters lead to an initial nonlinear estimator $g(y)$.
2) Initialize the inverse filter $\mathbf{f}_0 = [0, \cdots, 1, \cdots, 0]$ and the smoothing parameter $0.8 < \gamma < 0.95$.
3) For $k = 0$ to $m-1$:

   3.1. obtain the deconvolved output $\mathbf{y}_k = \mathbf{z} * \mathbf{f}_k$;
   3.2. recompute the posterior probabilities using (3) and (4);
   3.3. update the signal model according to (15) and (16);
   3.4. obtain a new signal estimate: $\hat{\mathbf{x}}_k = g(\mathbf{y}_k)$;
   3.5. reestimate the cross-correlation vector $\mathbf{g}$;
   3.6. obtain a new deconvolution filter $\mathbf{f}_{k+1}$ by solving (9);

   end.

IV. Simulation Results

In this section, we evaluate the performance of our algorithm using a synthetic signal of 500 samples (sampling period = 2 ms), generated according to the BG model [1], with $\lambda = 0.1$ and $\sigma^2_x = 10$. The BG input signal was convolved with a fourth-order nonminimum-phase ARMA wavelet, shown in Fig. 1(a), with transfer function given by

$$H(z) = \frac{-0.76286 + 1.5884z^{-1} - 0.82356z^{-2} + 0.000222419z^{-3}}{1 - 2.2633z^{-1} + 1.7734z^{-2} - 0.49803z^{-3} + 0.045546z^{-4}}. \tag{18}$$

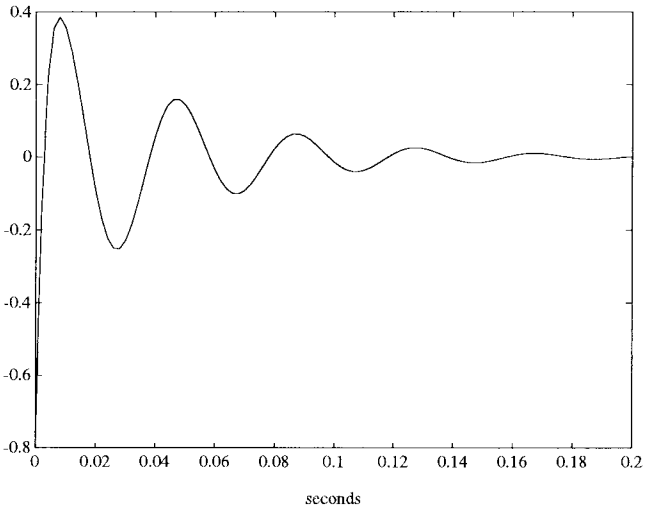

(a)

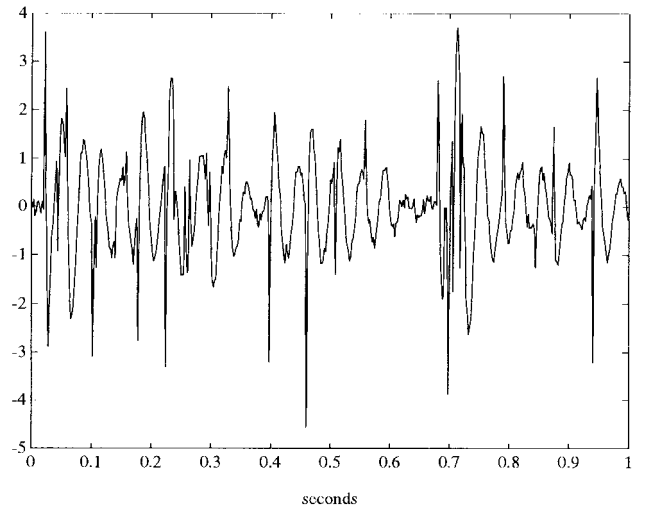

(b)

Fig. 1. (a) Fourth-order ARMA wavelet and (b) synthetic seismic data (SNR = 20 dB).

Finally, white Gaussian noise was added to produce the synthetic seismic data shown in Fig. 1(b) (SNR = 20 dB).

A deconvolution filter with 25 coefficients was used, with its central tap initialized to one. To apply the proposed method, we initialize the mixture parameters with the following values: $\pi_1 = \pi_2 = 0.5$, $\sigma^2_1 = \sigma^2_z/2$, and $\sigma^2_2 = 2\sigma^2_z$, where σ^2_z is the variance of the observations. Finally, for this example, we select $\gamma = 0.9$.

Fig. 2(a) and (b) show the estimated sparse sequence obtained with the proposed method (after 100 iterations) and with Godfrey's method (after ten iterations), respectively. The circles depict the true spikes of the BG signal, and the delay between the input signal and the estimate has been artificially removed. We see that the proposed method obtains a very accurate estimate, while Godfrey's method tends to underestimate the small reflectors. On the other hand, considering that the computational cost per iteration for both methods is roughly the same, our procedure entails a noticeable increase in computational complexity in relation to Godfrey's deconvolution procedure.

To explain these differences, Fig. 3 compares the nonlinear estimator used in the proposed method, while the algorithm proceeds, and the one used in Godfrey's method. Our method starts with a function almost linear; the updating procedure for the mixture parameters modifies the estimator, and after convergence, it yields a reasonable

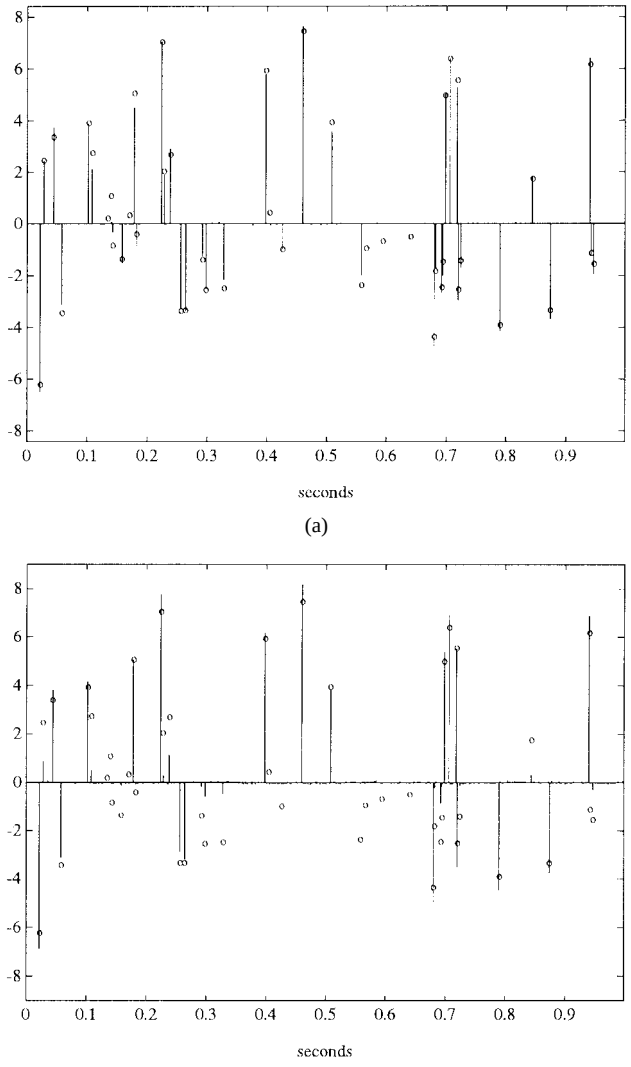

Fig. 2. Sparse sequence estimated with the (a) proposed method and with (b) Godfrey's method. Circles depict true spikes.

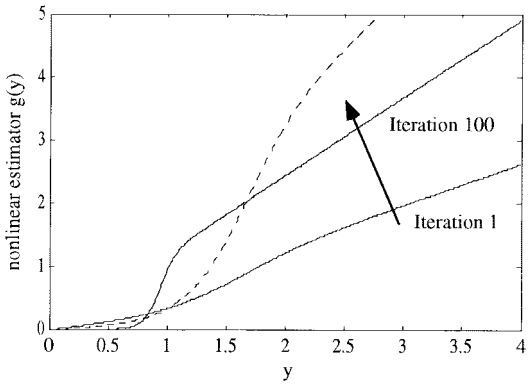

Fig. 3. Zero-memory nonlinearity for the proposed method (solid line) at iterations one and 100 (final result) and for Godfrey's method (dashed line). Input and output are normalized by the standard deviation.

nonlinear mapping. On the other hand, the fixed nonlinear estimator used in Godfrey's method is much more aggressive in the sense of suppressing the smaller peaks: this improves the convergence rate but leads to worse estimates.

Finally, Fig. 4(a) and (b) illustrate the evolution of the mixture parameters versus the number of iterations. Their final values (after

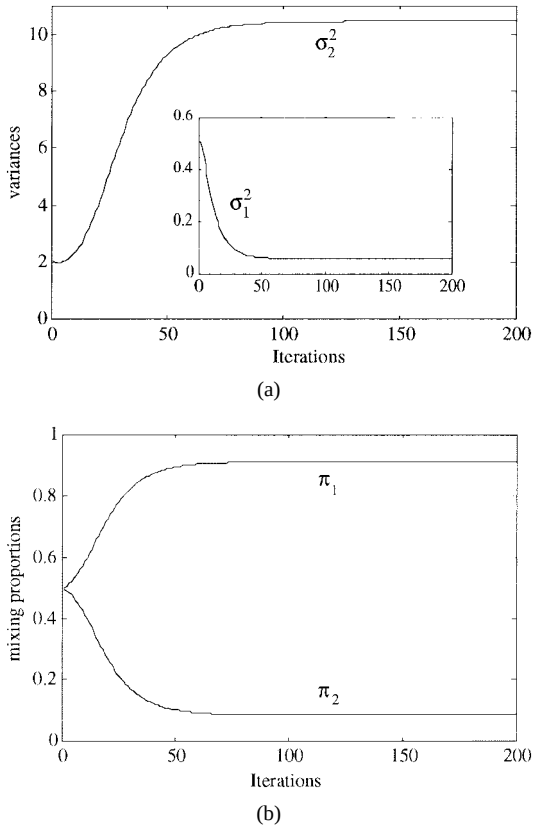

Fig. 4. Evolution of the Gaussian mixture parameters versus number of iterations: (a) variances and (b) mixing proportions.

iteration 100) are $\pi_1 = 0.91$, $\pi_2 = 0.09$, $\sigma_1^2 = 0.06$, and $\sigma_2^2 = 10.47$, which indicate that the proposed updating procedure approaches the correct values defining the input BG model.

V. Conclusions

This paper has presented a new Bussgang-type algorithm for blind deconvolution of seismic signals. An improvement and novelty in comparison with other Bussgang approaches is the use of an updating procedure for the parameters defining the nonlinear estimator (based on a Gaussian mixture model for the reflectivity). This procedure avoids an empirical selection of the hyperparameters that define both the pdf of the input signal and the nonlinear estimator. The proposed algorithm is able to find an appropriate distribution (belonging to a parametrized family of Gaussian mixtures) for modeling the input signal or, equivalently, it can select a zero-memory nonlinearity to estimate the reflectivity sequence. It has been shown that this technique achieves better estimates than Godfrey's method, but with a higher computational cost.

References

[1] J. M. Mendel, *Maximum Likelihood Deconvolution.* New York: Springer, 1990.
[2] F. Champagnat, Y. Goussard, and J. Idier, "Unsupervised deconvolution of sparse spike trains using stochastic approximation," *IEEE Trans. Signal Processing*, vol. 44, pp. 2988–2998, Dec. 1996.
[3] R. Godfrey and F. Rocca, "Zero memory nonlinear deconvolution," *Geophys. Prospecting*, vol. 29, pp. 189–228, 1981.
[4] S. Haykin, *Blind Deconvolution.* Englewood Cliffs: Prentice-Hall, 1994.
[5] D. Donoho, "On minimum entropy deconvolution," in *Applied Time Series Analysis II*, D. Findley, Ed. New York: Academic, 1981, pp. 556–608.

[6] I. Santamaría-Caballero, C. J. Pantaleón-Prieto, and A. Artés-Rodríguez, "Sparse deconvolution using adaptive mixed-Gaussian models," *Signal Process.*, vol. 54, pp. 161–172, 1996.
[7] A. P. Dempster, N. M. Laird, and D. B. Rubin, "Maximum likelihood from incomplete data via the EM algorithm," *J. Roy. Stat. Soc.*, vol. B-39, no. 1, pp. 1–37, Jan. 1977.

Scatterometer Observations of Seasonal Backscatter Variation Over Tropical Rain Forest

Iain H. Woodhouse, Joost J. van der Sanden, and Dirk H. Hoekman

***Abstract*—A strong correlation between the C-band ERS-1 windscatterometer (WSC) backscatter and local precipitation in Guyana has been observed. The effect on the correlation of incidence angle and local time is also examined. Characterizing such fluctuations may be useful for precise calibration of active microwave instruments.**

***Index Terms*—Calibration, radar cross sections, radar terrain factors, remote sensing, spaceborne radar, tropical regions.**

I. Introduction

Precise calibration of spaceborne radar instruments [synthetic aperture radar (SAR) and scatterometers] is difficult to achieve using prelaunch calibration alone so extensive postlaunch calibration campaigns are often carried out shortly after launch of a new instrument. One approach to calibration is to use the signatures of distributed targets of known radar cross section (RCS), such as extensive forests or agricultural fields. The assumption is that the area in question is uniform and that its average RCS for the particular radar configuration and time of year is known. As well as providing a calibration methodology for large footprint sensors [such as windscatterometers (WSC's)], this approach has been useful in determining relative calibration errors within higher resolution imagery and has been proposed for absolute calibration of SAR images ([1] and references therein).

Of the potential calibration sites, tropical rain forests, such as the Amazon and the Congo forests, show remarkably stable RCS over a large area and extended time periods. However, these regions do exhibit some degree of spatial and temporal variability that, if unaccounted for, can lead to biases and increased uncertainty in the calibration of the radar instrument. Seasonal variability has been included in previous calibration studies (e.g., [2] and [3]) but only as a seasonally fixed response and has not yet been directly related to any ground parameter. Characterizing such fluctuations as a function of measurable ground parameters could be of great benefit to the calibration of active microwave instruments, allowing for distinction between the seasonal variations in the forest and slow variations of the system gain.

This paper presents data that shows monthly scale correlations of ERS WSC RCS with precipitation for an area centered on Mabura Hill, Guyana. The results are compatible with other observations of high-resolution SAR.

Manuscript received October 22, 1997; revised June 1, 1998.

The authors are with the Department of Water Resources, Wageningen Agricultural University, 6709 PA Wageningen, The Netherlands (e-mail: i.h.woodhouse@dundee.ac.uk).

Publisher Item Identifier S 0196-2892(99)00840-2.

II. Test Region

Mabura Hill is situated at approximately 5° N and 59° W—about 250 km south of Guyana's capital, Georgetown. The site covers roughly 250 000 hectares (50 × 50 km) of tropical rain forest that has some areas undergoing industrial selective logging as well as an area set aside as an ecological reserve. Rainfall measurements are recorded at the Mabura Hill Weather Station, located at a clearing in the forest of approximately 50 × 50 m and operated by the Tropenbos Foundation [4].

Seasonal change in Guyana is related to north–south movements of the intertropical convergence zone (ITCZ), which influences mainly annual rainfall distribution. A long wet season occurs from May to August and a short wet season from December to February. The remaining periods are dryer, with October generally being the driest month. Most rainfall falls in the late afternoon and early evening, which is related to instability in the atmosphere caused by irradiation.

III. Scatterometer Data

The ERS WSC's are mounted on the ESA ERS-1 and 2 platforms [5] and were designed to obtain information on wind speed and direction over the sea surface, although measurements are also made over land.

The instrument consists of three antennas producing three beams looking 45° forward, sideways and 45° backward with respect to the satellite's orbit direction. These beams continuously illuminate a 500-km wide swath as the satellite moves along its orbit with local incidence angles across the swath ranging from 18 to 59°.

The spatial resolution of the instrument is in the order of 50-km along and across track with an estimated radiometric stability of <0.22 dB [3]. The operating frequency is 5.3 GHz (C-band) with vertical transmit and receive (VV) polarization. WSC measurements have been made nearly continuously since July 1991 and are referred to throughout this communications in terms of $\gamma = \sigma^0 / \cos\theta_i$, where θ_i is the local incidence angle (assuming a smooth earth).

IV. Results and Discussion

A. Background

An investigation of the WSC backscatter properties over the Mabura Hill test site showed an initial correlation between the averaged monthly backscatter and the total monthly precipitation measured at the test site over a period of two years [6]. Fig. 1 shows these results for two incidence ranges for 1992 and 1993. Such a correlation would be expected since the presence of additional water in the forest canopy or ground (as surface water or as increased moisture content) would result in an increased RCS.

In previous studies [7], individual rain cells have been identified in high-resolution ERS SAR data, showing storm clouds resulting in attenuation in the order of 2.5 dB, while behind the cloud, the increased soil or vegetation humidity increases the backscatter by about 0.6 dB. Another study, based on ERS-1 SAR data, has observed considerable temporal change (ca., 1 dB) in the RCS for discrete regions of intact forest in the Mabura Hill region, apparently related to the seasonal variation in gravimetric water content of full grown leaves (ca., ± 0.1 gg^{-1}) [8].